MEASURING FRICTION LOSSES OF LARGE-ANGLE POST-TENSIONED CONCRETE WALLS

Jongkwon Choi, The University of Texas at Austin, Austin, TX
Clint R. Woods, Walter P Moore, Houston, TX
Trevor D. Hrynyk, PhD, The University of Texas at Austin, Austin, TX
Oguzhan Bayrak, PhD, PE, The University of Texas at Austin, Austin, TX

ABSTRACT

Friction losses in post-tensioned concrete structures can account for more than 50 % of the losses developed during prestressing operations. Accurate friction loss estimation is necessary for safe and economic design. Existing code equations and coefficients were developed in the 1950's and first introduced in the ACI 318 guidelines in 1963, and no significant changes have been made since. Further, these equations were derived based on small angle assumptions and do not consider effects related to strand interaction for multi-strand post-tensioning applications. The use of these equations in large-angle post-tensioning applications, such as hoop post-tensioning in cylindrical structures, may lead to unrealistic estimations of friction losses. In this paper, friction loss measurements were compared with estimated losses computed on the basis of current theory. Three 90-degree wall specimens were fabricated, each comprised of four evenly-spaced ducts that contained multiple strands. To evaluate friction losses, both live-end and dead-end loads were measured over the course of the stressing operations. Anticipated friction losses were on the order of about 33 %; however, the measured losses were found to range from 40 to 60 %. The large-angle configuration and strand interaction within the ducts were identified as probable causes for the larger-than-anticipated friction loss results obtained.

Keywords: Friction loss, Curvature coefficient, Large-angle post-tensioned, Strand interaction, Binding effect, Squeezing effect, Elongation

INTRODUCTION

The safe and reliable construction of the post-tensioned concrete structures requires accurate estimation of the force distribution in the tendons at the initial stages (immediately after prestress transfer) and under service conditions. At the initial stage, major factors affecting prestress losses are friction loss, anchorage slip, and elastic shortening of the concrete. Friction loss occurs due to an interaction between strands and surrounding materials, and induces a gradual force reduction along the tendon. Therefore, the effective prestressing forces along a post-tensioning structure are a function of the distance from the jacking end. Furthermore, friction losses could account for more than 50 % of the total losses developed during prestressing operations. In some extreme cases, serviceability requirements of concrete stress specified in code provision could not be satisfied due to friction losses.

Friction losses may consist of both intended curvature of the tendons (that is curvature friction) and unintended misalignment of the tendons (that is wobble friction). Both curvature and wobble frictions are dependent on the properties and condition of materials such as prestressing steels, ducts, usage of lubrications, and the hardness difference between the prestressing steel and duct, and surface condition (for example, rust formation on the prestressing steel or the metal duct). Based on previous tests and experiences, recommended curvature and wobble coefficients have been provided in various code provisions and used as the basis for calculating expected elongations and friction losses of post-tensioned structures.

There are several additional factors that could also contribute to friction losses. The tendon profiles within structural components such as beams and slabs are generally placed in a manner that will compensate for the external bending moment acting along the structure with the internal moment generated by the tendon profiles. Therefore, a wave-shape of a tendon profile would be expected for multi-span post-tensioning structures. To calculate the friction losses over the lengths of the tendon provided in such structures, angular changes are calculated for each segment and accumulated along the structures. One of the primary assumptions is that the prestressing steels and ducts are continuously in contact with each other along the length of structures. In reality, however, for rectilinear and straight beam structures, the contact between prestressing steels and ducts are minimal in the vicinities of the each inflection points, since the inside area of ducts are typically more than two times the area of the strands as per code recommendations[1,2]. In contrast, prestressing steels are in near-continuous contact with the ducts comprising cylindrical structures such as silos, bins, storage containers, and nuclear containments which have a single curvature along the circumferential direction.

The curvature coefficients in various codes are the product of a physical coefficient of friction (μ_o) and a squeezing factor which is owing to a circular shape of duct cross-section. During the prestressing operation, prestressing steels are stacked toward the direction of a lateral pressure owing to the deviation of the tendon. It is generally believed that the squeezing factor is dependent on the degree of filling of the ducts. There is no research available to definitively quantify the squeezing effect; however, the provisions of the *fib* Model Code 2010[3] does specify the squeezing factor as 1.3 to 1.35 for 50 to 60 % occupancy of strands within ducts.

Generally, curvature coefficients provided in many code provisions inherently take into account influences associated with the squeezing effect.

Prestressing steels can be placed within ducts using either pull-through or push-through methods.[4,5] Pull-through methods are typically used for special structures such as long span cast-in-place bridges, buildings, and nuclear containment structures. In most cases, the entire strand bundle is pulled through the duct using a winch with a steel cable. Push-through methods are more widely used for tendon placements because it is more economic and flexible method for general post-tensioning structures.[6] During the tendon installation using either methods, the arrangement of prestressing steels may be subjected to change along the length of structures due to the deviation of the tendon. This could create some twisted strands and induce strand interactions which could result in larger friction losses.[7,8]

An experimental program to investigate the behavior of curved post-tensioned concrete wall assemblies was performed and it was found that the measured friction losses were on the order of 38 to 43 % higher than the expected friction losses calculated on the basis of current code provisions.[9] The aforementioned additional factors are typically negligible or are inherently considered in friction coefficients for general post-tensioning members with relatively small angular changes. However, it is likely that such friction factors may contribute significantly to the friction losses of large-angle post-tensioned structures. In this paper, the friction losses and the actual curvature coefficients were evaluated on the basis of measured loads and probable causes of larger curvature coefficients are discussed.

BACKGROUND

FRICTION LOSS

The main sources of friction losses in post-tensioning structures are intended tendon profile of ducts (that is curvature effect, μ) and unintended deviation of ducts due to concrete placement and vibration (that is wobble or length effect, κ).[10] The prestressing forces acting at a distance x from the jacking point, considering both curvature and wobble effects, can be estimated using Equation (1).[11]

$$P_b = P_a \cdot e^{-(\mu\alpha+\kappa x)} \quad (1)$$

where, P_a = applied prestressing force at the live-end
P_b = applied prestressing force at the angle of α
μ = friction coefficient
α = angular change of tendon (radian)
κ = wobble coefficient (ft^{-1})
x = length of tendon (ft)

In typical post-tensioned concrete structures (especially, multi-span structures), the tendon profiles are assumed as a combination of parabolic and inverse parabolic curves. The entire

structure is subdivided into several segments with respect to vertices and inflection points (Fig. 1). Then the angular deviations of the tendon for each segment are calculated using Equation (2).[11] To obtain the total angular deviation (α) at a distance x, the cumulative angular deviation (θ_i) for each segment, from the jacking-end (live-end) to the fixed-end (dead-end), is required.

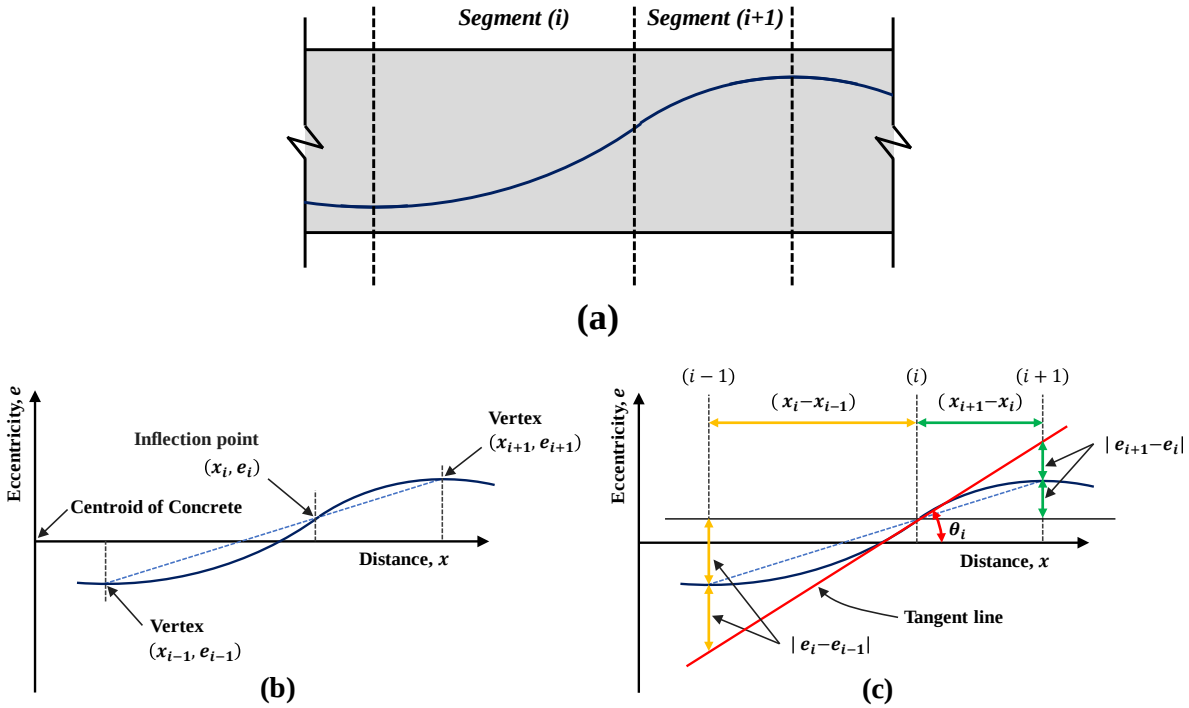

Fig. 1 (a) Partial section of a post-tensioned concrete structure (b) Location of vertexes and inflection points, and (c) Tangent line at an inflection point[12]

$$\theta_i = \tan^{-1}\left[\frac{2 \times |e_i - e_{i-1}|}{x_i - x_{i-1}}\right] = \tan^{-1}\left[\frac{2 \times |e_{i+1} - e_i|}{x_{i+1} - x_i}\right] \quad (2)$$

where, θ_i = angular deviation of segment (i)
e_i = eccentricity from centroid of concrete at section (i)
x_i = distance from jacking end at section (i)

FRICTION COEFFICIENT

Curvature and wobble coefficients for post-tensioning tendons have been given as ranges of values in various codes and provisions, as shown in Table 1 through Table 7. Friction losses were first introduced in ACI 318 in 1963 and, at that time, only the curvature and wobble coefficients for bonded post-tensioning system with metal sheathing were provided (refer to Table 1). A range of observed friction coefficients and suggested design values were given for three types of prestressing steels that were widely used for the post-tensioning system. The use of post-tensioning increased rapidly during the late 1960s and 1970s as advantages of the system were demonstrated. As a result, friction coefficients existing at that time were modified

and new friction coefficients for unbonded tendons were added in ACI 318 in 1971, and remained in ACI 318 until 2008 (refer to Table 2). After 2011, the friction coefficients were omitted from the ACI 318 provisions and designers were referred to the Post-Tensioning Manual[6]. The friction coefficients in the Post-Tensioning Manual were given for different types of ducts with 7-wire strands, as shown in Table 3.

Table 1 Friction coefficients in ACI 318-63[1]

Type of steel	Usual range of observed values		Suggested design values	
	κ	μ	κ	μ
wire cables	0.0005-0.0030	0.15-0.35	0.0015	0.25
high strength bars	0.0001-0.0006	0.08-0.30	0.0003	0.2
galvanized strand	0.0005-0.0020	0.15-0.30	0.0015	0.25

Table 2 Friction coefficients in ACI 318-71~08[1]

			Wobble coefficient, κ	Curvature coefficient, μ
Grouted tendons in metal sheathing		Wire tendons	0.0010-0.0015	0.15-0.25
		High strength bars	0.0001-0.0006	0.08-0.30
		7-wire strand	0.0005-0.0020	0.15-0.25
Unbonded tendons	Mastic-coated	Wire tendons	0.001-0.002	0.05-0.15
		7-wire strand	0.001-0.002	0.05-0.15
	Pre-greased	Wire tendons	0.003-0.002	0.05-0.15
		7-wire strand	0.003-0.002	0.05-0.15

Table 3 Friction coefficients in Post-tensioning manual[6] (referenced in ACI 318-11 and 14[1])

Type of duct	Range of values		Recommended for calculations	
	μ	κ	μ	κ
Flexible tubing non-galvanized	0.18-0.26	0.0005-0.0010	0.22	0.00075
Flexible tubing galvanized	0.14-0.22	0.0003-0.0007	0.18	0.0005
Rigid thin wall tubing non-galvanized	0.20-0.30	0.0001-0.0005	0.25	0.0003
Rigid thin wall tuning galvanized	0.16-0.24	0-0.0004	0.2	0.0002
Greased and wrapped	0.05-0.15	0.0005-0.0015	0.07	0.001

AASHTO LRFD specifications[2] contains a table of friction coefficients suggested for various types of tendons and ducts for bridge construction (refer to Table 4). It should be noted that the values for friction coefficients in AASHTO LRFD specifications were found to be reasonably accurate for tendons comprised of 12 strands of 0.5-in. diameter in a 2.625-in. diameter galvanized metal sheathing.[2] On the basis of the experience of job-site tests, the values in Table 4 have deemed to be somewhat conservative for both larger tendons and larger

duct diameters.[2] However, In the Caltrans Bridge Design Specifications,[13] the friction coefficients presented in the AASHTO LRFD specifications were adapted and modified such that the friction coefficients for galvanized metal sheathing with wire or strand were subdivided into four categories depending on the length of duct (refer to Table 5). Further, the Caltran Specifications also suggested that lubrication should be used for tendons longer than 1200 ft.

Table 4 Friction coefficients in AASHTO LRFD Bridge Design Specifications[2]

Type of steel	Type of duct	κ	μ
Wire or strand	Rigid and semi-rigid galvanized metal sheathing	0.0002	0.15-0.25
	Polyethylene	0.0002	0.23
	Rigid steel pipe deviators for external tendons	0.0002	0.25
High-strength bars	Galvanized metal sheathing	0.0002	0.3

Table 5 Friction coefficients in Caltrans Bridge Design Specifications

Type of steel	Type of duct	κ	μ **
Wire or strand	Rigid and semi-rigid galvanized metal sheathing		
	1-600 feet	0.0002	0.15
	600-900 feet	0.0002	0.2
	900-1200 feet	0.0002	0.25
	>1200 feet	0.0002	0.25*
	Polyethylene	0.0002	0.23
	Rigid steel pipe deviators for external tendons	0.0002	0.25*
High-strength bars	Galvanized metal sheathing	0.0002	0.3

* Lubrication will probably be required.
** Add effect of horizontal curvature if any.

ACI 343R-95[11] contains more detailed friction coefficients considering different types of tendons and sheathing for concrete bridges (refer to Table 6). Friction coefficients for flexible metal sheathing were additionally provided in ACI 343R-95, while friction coefficients in AASHTO LRFD were focused on rigid galvanized metal sheathing. Furthermore, friction coefficients for unbonded tendons such as pregreased tendons and mastic-coated tendons that were given in ACI 318 were also provided in addition to bare tendons in metal ducts.

Table 6 Friction coefficients in ACI 343R-95[11]

Type of tendons and sheathing	Wobble coefficient, κ		Curvature coefficient, μ
	per ft	per m	
Tendons in flexible metal sheathing			
- wires	0.0010-0.0015	0.0033-0.0049	0.15-0.25
- 7-wire strands	0.0005-0.0020	0.0016-0.0066	0.15-0.25
- high-strength bars	0.0001-0.0006	0.0003-0.0020	0.08-0.30

Tendons in rigid and semi-rigid galvanized - 7-wire strands	0.0002	0.00066	0.15-0.25
Pregreased tendons - wires and 7-wire strands	0.0003-0.0020	0.0010-0.0066	0.05-0.15
Mastic-coated tendons - wires and 7-wire strands	0.0010-0.0020	0.0033-0.0066	0.05-0.15

ACI 423.10R-16 "Guide to Estimating Prestress Loss" which provides comprehensive friction coefficients (refer to Table 7) for almost all available combinations of materials (e.g., different types of prestressing steels, different types of ducts, and lubrication of strands that are currently employed in prestressed concrete construction).

Table 7 Friction coefficients in ACI 423.10R-16 [12]

Type of prestressing steel	Corrugated metal duct		Corrugated plastic duct		Smooth steel pipe		Smooth plastic pipe		No duct plastic sheathing	
	μ	κ, ft^{-1} (m^{-1})	μ	κ, ft^{-1} (m^{-1})	μ	κ, ft^{-1} (m^{-1})	μ	κ, ft^{-1} (m^{-1})	μ	κ, ft^{-1} (m^{-1})
Strand	0.15-0.25	0.00005-0.0003 (0.0002-0.0010)	0.10-0.14	0.000005-0.0003 (0.0002-0.0010)	0.25-0.30	0	0.10-0.14	0	-	-
Strand in precast elements and constant curvature tendons	0.15-0.25	0.00005-0.0003 (0.0002-0.0010)	0.10-0.14	0.000005-0.0003 (0.0002-0.0010)	-	-	-	-	-	-
External tendons, bare dry strand	-	-	-	-	0.25-0.30	0	0.12-0.15	0	-	-
Lubricated strand	0.12-0.18	0.00005-0.0003 (0.0002-0.0010)	-	-	0.25-0.30	0	-	-	-	-
Strand coated and extruded*	0.01-0.05	0.00005-0.0003 (0.0002-0.0010)	0.01-0.05	0.00005-0.0003 (0.0002-0.0010)	0.01-0.05	0	0.01-0.05	0	0.01-0.07	0.00005-0.0003 (0.0002-0.0010)
Bars, deformed, smooth, and round	0.30	0-0.0002 (0-0.0007)	0.30	0-0.0002 (0-0.0007)	-	-	-	-	-	-

* Post-tensioned coating in accordance with the performance specification (PTI M10.3-00).

Even though ranges of recommended friction coefficients can be found from various standards and technical documents, job-specific friction coefficients based on experimental data for the actual materials specified and used are likely to yield superior results in most cases and will inherently account for noted uncertainties associated with friction loss estimates.

JACKING FORCE AND TENDON ELONGATION

To ensure the appropriate force distribution considering friction losses, jacking forces and tendon elongations are typically monitored over the course of the prestressing operation. The jacking forces can be simply calculated using pump pressure and an effective area of the pump.

Cooley (1953)[14] derived a theoretical elongation equation for multi-span post-tensioning systems. The theoretical elongation is a function of jacking forces and several other variables such as curvature coefficients, wobble coefficients, and the lengths of tendons. The measured tendon elongations are compared with theoretical tendon elongations[6] for the purpose of verifying that elongation tolerances specified in various code provisions are satisfied (refer to Table 8).[12] If measured tendon elongations exceed the tolerance limits, a lift-off test should be performed from the dead-end anchorage to ensure appropriate force transfer. However, the lift-off test is not a routine procedure due to the fact that the test requires special equipment and procedures to assure construction safety.[6,15] Therefore, if both jacking forces and tendon elongations are satisfying the tolerances, the dead-end forces are typically not measured.

Table 8 Tolerances for the correlation between the expected and measured elongations in selected codes (ACI 423.10R-16[12])

Code	**Tolerance in elongation Expected versus measured, percent**
ACI 318-11	± 7 percent
AASHTO (1989)	± 5 percent on individual tendon based on friction coefficients confirmed with liftoff tests, and material properties of the actual materials used
AASHTO (2011)	± 5 percent for tendon length over 50 ft (15 m) ± 7 percent for tendon length 50 ft (15 m) or less
Eurocode EN 13670:2009	± 5 percent for the total force at a section ± 15 percent for an individual tendon
CEB-FIP model code (Comité Euro-International du Béton 2010)	Tendon L > 50 ft (15 m): ±10 percent for a particular tendon ±5 percent for all tendons in a section Tendon L ≤ 50 ft (15 m): ±15 percent for a particular tendon ±7 percent for all tendons in a section

EXPERIMENTAL PROGRAM

TEST SPECIMENS AND VARIABLES

Three 90-degree post-tensioned concrete wall assemblies were fabricated, each comprised of four evenly-spaced ducts that contained multiple strands. The specimens were designed such that the global behavior approximately represented the behavior of a full cylindrical post-tensioned concrete structure. Four ducts were evenly-spaced over the height of the wall assemblies to make a near-uniform distribution of the lateral forces owing to the curved geometry of specimens. The centroid of the ducts was approximately located in the mid-height of the cross-section of the wall assemblies, and all ducts were slightly shifted toward the outer surface of the wall such that the centroid of the strands are located at the centroid of the wall cross-section. In this way, the out-of-plane (global) bending owing to the eccentricity of strands could be eliminated or minimized during the stressing operation. As shown in Fig. 2, the offsets

of the ducts were 0.25 in. for Specimen 1 and 0.75 in. for Specimen 2 and Specimen 3. Design and analysis methods for vertical and horizontal reinforcement are presented elsewhere.[9,16]

ASTM A 513 steel tubes with 2 in. and 4 in. outside diameter were used to accommodate the dimension of the specimens. Steel tubes were pre-bent in 90-degree angles with a 7 ft radius for the smaller specimen (Specimen 1) and with a 14 ft radius for the larger specimens (Specimen 2 and 3). The sectional dimension of ducts and the number of strands per each duct were determined to satisfy ACI 318-14[1] requirements; an inside cross-sectional area of ducts should be at least two times the cross-sectional area of the prestressing steel. The properties of post-tensioning ducts used are presented in Table 9.

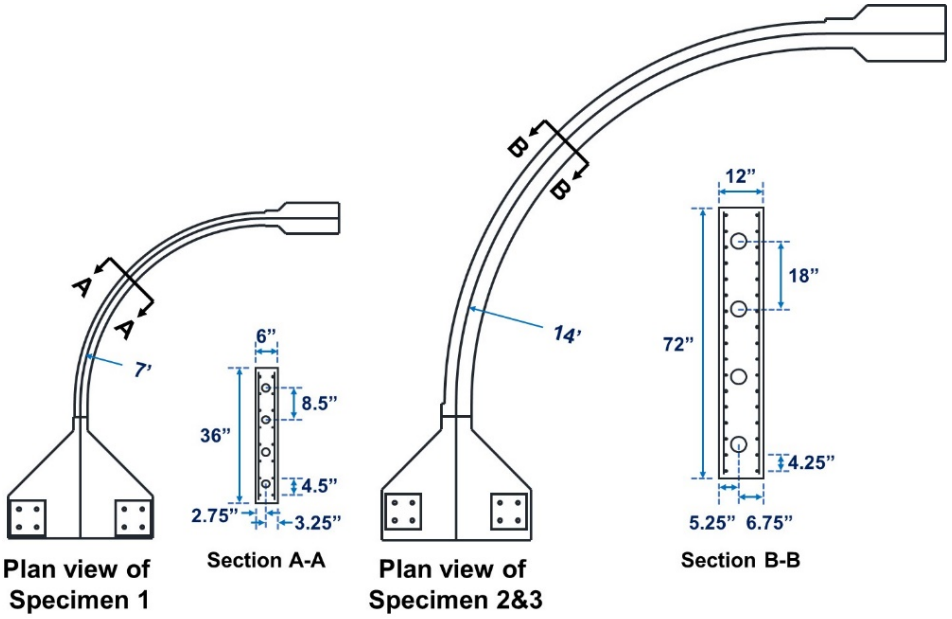

Fig. 2 Summary of specimen dimensions

Table 9 Properties of post-tensioning ducts

	Unit	Specimen 1	Specimen 2	Specimen 3
Type of material	-	ASTM A513 Type 5		
Outside diameter	in.	2	4	4
Thickness	gage (in.)	14 (0.083)	14 (0.083)	13 (0.095)
Bend radius*	ft	7	14	14
Number of strands per duct	-	4	19	19
$A_{inside}/A_{strands}$**	-	2.97	2.79	2.75

* Measured from the centroid of ducts

** A_{inside} = inside cross-sectional area of the duct, $A_{strands}$ = total cross-sectional area of the prestressing strand

Strand properties for each specimen are presented in Table 10. Four 0.6 in. 7-wire strands were provided for each duct comprising Specimen 1 and nineteen 0.6 in. 7-wire strands were provided for each duct comprising Specimen 2 and Specimen 3. Individual strands or bundled strands were placed within the duct using the push-through method. No lubricants were used for the strands in this test program. The number of strands for each inserting sequence is summarized in Table 11.

Table 12 shows a summary of the concrete material properties for the three specimens. The compressive strength of Specimen 1 was lower than that of Specimen 2 and Specimen 3. Though the compressive strength of Specimen 1 satisfied the minimum requirement of compressive strength at stressing (3000 psi) as specified in the Post-Tensioning Manual,[6] the design concrete strength for Specimen 2 and Specimen 3 were increased due to the fact that the anticipated prestressing forces for Specimen 2 and Specimen 3 were estimated to be more than four times the measured prestressing forces obtained for the smaller-scale Specimen 1.

Table 10 Strand properties from manufacturer

	Unit	Specimen 1	Specimen 2	Specimen 3
Area	$in.^2$	0.222	0.218	0.218
Yield load	lbf	56769	56471	56800
Ultimate breaking load	lbf	62715	62128	61600
Ultimate strength, f_{pu}	ksi	283	285	283
Modulus of elasticity, E_p	ksi	28300	29000	28800
Ultimate elongation	%	7.77	7.77	6.63

Table 11 Number of strands per each inserting sequence

Specimen	Duct*	Number of strands per each inserting sequence
Specimen 1	Duct 1	4
	Duct 2	4
	Duct 3	4
	Duct 4	4
Specimen 2	Duct 1	10+9
	Duct 2	12+5+2
	Duct 3	5+12+2
	Duct 4	18+1
Specimen 3	Duct 1	Individual strands
	Duct 2	Individual strands
	Duct 3	Individual strands
	Duct 4	10+9

*Note: The ducts were numbered from the top, therefore, duct 1 is the first duct from the top.

Table 12 Properties of concrete for each specimen at structural test

Property	Unit	Specimen 1	Specimen 2	Specimen 3
Compressive strength, f_c'	ksi	3.010	6.800	5.560
Elastic modulus, E_c	ksi	3580	4910	5480
Poisson's Ratio, ν	ksi	0.18	0.2	0.22

TEST SETUP AND LOADING PROTOCOL

The live-end end blocks for all specimens were anchored to the strong floor with a total tie-down force of 240-kip while the rest of the structures were positioned on the two layers of polytetrafluoroethylene (PTFE) sheets creating a low-friction surface condition that permitted free movement over the course of the prestressing operation. As a result, all specimens were statically determinate with fixed-free boundary conditions.

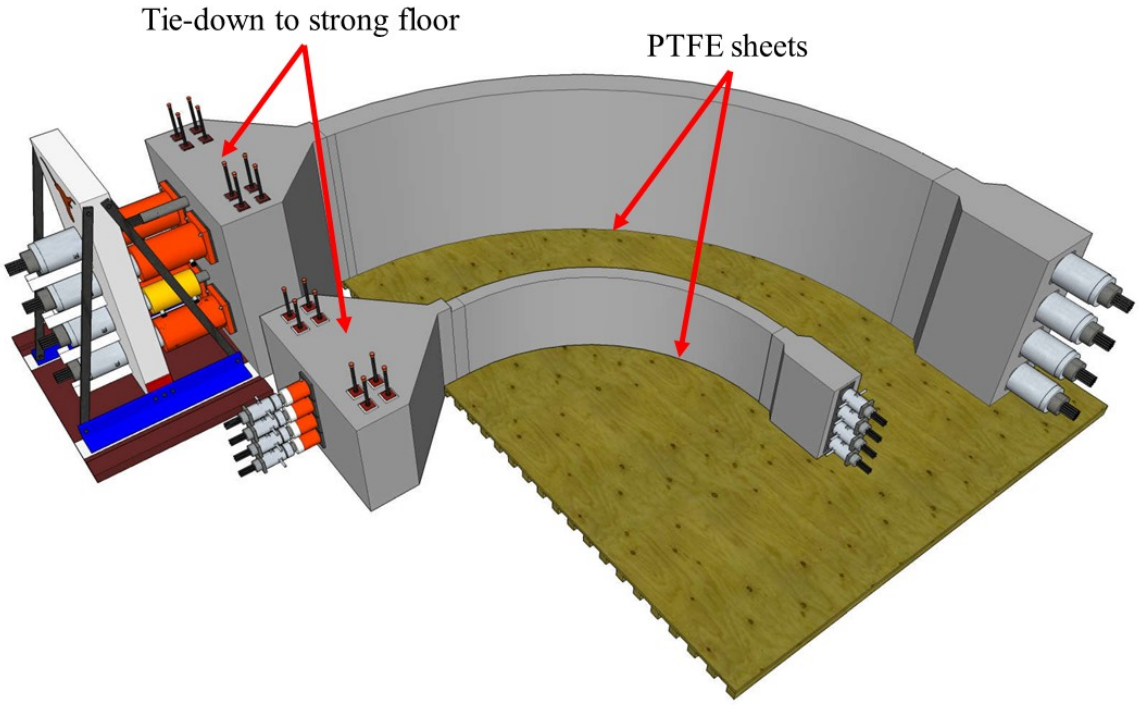

Fig. 3 Schematic size comparison between small and large specimens

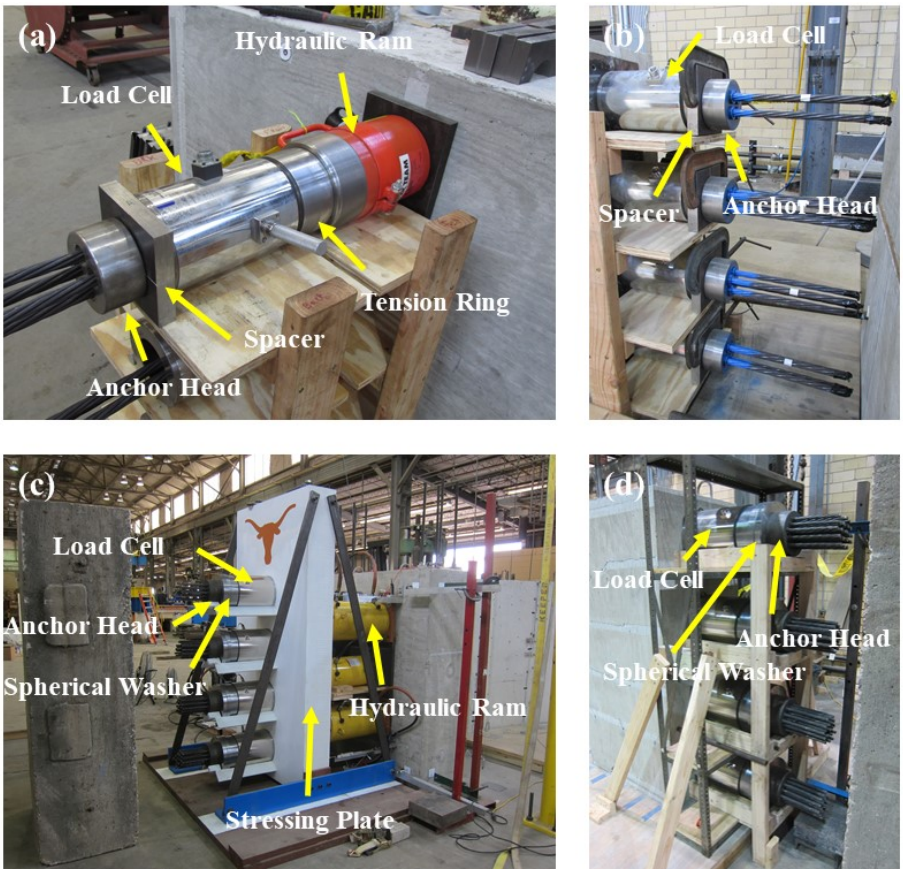

Fig. 4 Detail of test setup: (a) live-end block for Specimen 1, (b) dead-end block for Specimen 1, (c) live-end block for Specimen 2, and (d) dead-end block for Specimen 2

In an effort to evaluate the friction losses, prestressing strands were only stressed from live-end anchor block of each specimen. For the live-end of Specimen 1, a 120-kip hydraulic ram with 2-1/8 in. center hole and a load cell with 3-1/4 in. center hole were installed in a row on each duct as shown in Fig. 4 (a). Tension rings were placed between the load cells and the hydraulic rams, and spacers were placed between the anchor heads and the load cells for the precise alignment of load cells and rams. For the purpose of evenly distributing the loads amongst the tendons, individual strands were loaded approximately 1 to 2 kips using a monostrand hydraulic ram from both ends of Specimen 1 such that any existing slack was removed prior to the prestressing operation. For the live-end of Specimen 2 and Specimen 3, a 10-in. thick steel plate was used as a stressing plate. Four 800-kip hydraulic rams were placed between the live-end anchor block and the stressing plate, and were used to push the stressing plate away from the live-end anchor block (Fig. 4 (c)). A 1000-kip capacity load cell was installed on each strand group to monitor the prestressing load over the course of the prestressing operation. To provide same loads to each strand group, slack removal was also performed for both ends of each specimen prior to the prestressing operation. For the purpose of measuring friction losses of all specimens, load cells were also installed for each strand group on the dead-end anchor blocks (Fig. 4 (b), (d)).[9]

All hydraulic rams for each specimen were connected to one pneumatic pump using a hydraulic manifold system. As a result, all tendons were stressed simultaneously and approximately at the same level of live-end loads over the course of the prestressing operation. Due to the simultaneous applied loads to all tendons, it is believed that the effect of the prestress loss owing to the elastic shortening of concrete was negligible. The prestressing wedges were installed on the anchor heads before the prestressing operation and the loads were applied monotonically. Thus, the prestress loss due to the wedge slips could be neglected from the friction loss calculations; however, the wedge slips should be taken into account to calculate measured tendon elongations.

Specimen 1 was loaded in 50-kip increments up to a load level of 350 kips. After surpassing an applied force of 350 kips, the specimen was subsequently loaded to the failure. Specimen 2 and Specimen 3 were loaded in a manner to that done for Specimen 1. The specimens were loaded in 100-kip increments up to a load level of 1,000 kips and from 1,000 kips to 2,000 kips, the load was increased in 200-kip increments. After surpassing the 2,000-kip load level, the specimen was loaded to failure. During the stoppages, the specimens were briefly inspected and pictures were taken. The friction losses were evaluated from 8 to 50 % of ultimate breaking strength (f_{pu}) of strands.

TEST RESULTS AND DISCUSSION

The length of tendons within the curved portion of each structure was 11 ft for Specimen 1 and 22 ft for Specimens 2 and 3, respectively. From Table 3 to Table 7, the range of wobble coefficients using 7-wire strands and rigid metal ducts were varying from 0 to 0.0002 ft^{-1} regardless of the length of tendons. Though the largest value (0.0002 ft^{-1}) within the recommended range of wobble coefficients was used for the friction loss calculations, the wobble effects contributed less than 1 % toward the total friction losses because of the short length of tendon. Thus, the wobble effects were neglected from the evaluation of test data.

FRICTION COEFFICIENTS

Equation (1) could be rearranged into Equation (3) to calculate friction coefficients of the test specimens. Wobble coefficient (K) was assumed zero and curvature coefficients for each tendon were evaluated using the measured loads. The curvature coefficients calculated using Equation (3) are summarized in Table 13.

$$\mu\alpha + \mathrm{K}x = \ln\frac{P_{live}}{P_{dead}} \tag{3}$$

where, P_{live} = load at live-end
P_{dead} = load at dead-end

Table 13 Summary of curvature coefficients

	Duct*	Number of strands per each inserting sequence	Average friction loss (%)**	Curvature coefficient	
				Average***	At $0.5f_{pu}$
Specimen 1	Duct 1	4	47.1	0.41	0.40
	Duct 2	4	44.2	0.37	0.41
	Duct 3	4	44.3	0.37	0.38
	Duct 4	4	49.8	0.44	0.40
Specimen 2	Duct 1	10+9	46.5	0.40	0.44
	Duct 2	12+5+2	47.4	0.41	0.45
	Duct 3	5+12+2	39.6	0.32	0.36
	Duct 4	12+7	45.9	0.39	0.43
Specimen 3	Duct 1	Individual strand	58.1	0.55	0.57
	Duct 2	Individual strand	58.8	0.57	0.58
	Duct 3	Individual strand	59.5	0.58	0.58
	Duct 4	10+9	44.3	0.37	0.40

* Note: The ducts were numbered from the top, therefore, duct 1 is the first duct from the top

** $\frac{P_{live}-P_{dead}}{P_{live}} \times 100$; P_{live} = Load at live-end, P_{dead} = Load at dead-end

*** Average curvature coefficient from $0.08f_{pu}$ to $0.50f_{pu}$

The anticipated friction losses using Equation (1) with the curvature coefficient of 0.25 were approximately 33 % for all specimens. However, as shown in Table 13, average friction losses for each duct were found to range from approximately 40 to 60 %, values which are approximately 20 to 80 % larger than the anticipated friction losses estimated on the basis of current provisions.

Though the properties of materials and inserting methods of all ducts in Specimen 1 were identical, the average curvature coefficients were found to vary from 0.37 to 0.44. Further, it was also found that as the load increased, the curvature coefficients were converged to approximately 0.40. The bundled strands with a different number of strands per each bundle were inserted into the ducts for Specimen 2. Duct 1, Duct 2, and Duct 4 in Specimen 2 showed a similar range of average curvature coefficients with Specimen 1; ranging from 0.39 to 0.41. The average curvature coefficient for Duct 3 in Specimen 2 was 0.32 which is lower than other ducts in Specimen 2. It is interesting to note that the curvature coefficients increased to approximately to 0.44 for Ducts 1, 2, and 4, and 0.36 for Duct 3, respectively, as the load level of the strands increased. Based on the average curvature coefficients obtained from the test results of Specimen 1 and Specimen 2, the curvature coefficients ($\mu = 0.36$ to 0.45) are 44 to 80 % higher than the curvature coefficients specified in the codes ($\mu = 0.25$).

Individual strands were inserted into the ducts for Duct 1, Duct 2, and Duct 3 in Specimen 3 and the average curvature coefficients were found to range from 0.55 to 0.58, which is approximately 28 % higher than the average curvature coefficients obtained from the bundled strands. However, the average curvature coefficient for Duct 4 in Specimen 3 in which the strand was inserted with the same number of bundles for Duct 1 in Specimen 2 was 0.37 and

this value is within the range of curvature coefficients of Specimen 1 and Specimen 2. A possible cause of the large friction losses and curvature coefficients is ascribed to the strand interaction induced by installation of individual strands. This concept is discussed in a later section of this paper.

Fig. 5 shows relationships between live-end and dead-end measured loads for each specimen. It should be noted that the load relationship for each specimen was near-linear as expected. The shaded areas are ranges of the expected live- and dead-end loads using curvature coefficients ranging from 0.15 to 0.25 and from 0.30 to 0.50 (0.30 to 0.60 for Specimen 3).

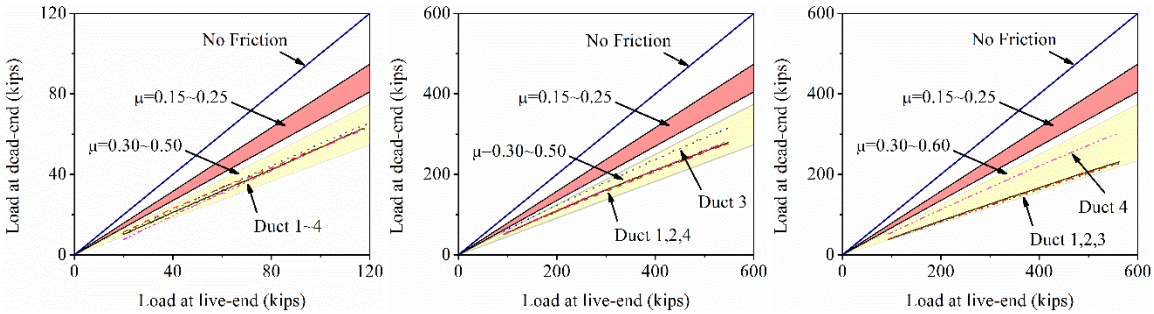

Fig. 5 Live and dead-end loads; (a) Specimen 1, (b) Specimen 2, and (c) Specimen 3

EFFECT OF SPECIMEN SIZE

If the curvature coefficient of Duct 3 in Specimen 2 is excluded, the average curvature coefficients for Specimen 1 and Specimen 2 were 0.40. At the ultimate load, the curvature coefficients were converging to 0.40 and 0.44, respectively. There are slight increases of the curvature coefficients for larger tendon radii. However, since the curvature coefficient of Duct 3 in Specimen 2 was lower than that of Specimen 1, it is believed that there was no specimen size effect apparent in the friction loss measurements. It is suspected that slight increases of the final curvature coefficients were attributed to the strand interaction due to the number of strands per each inserting method.

STRAND INTERACTION

As mentioned previously, the contact between prestressing strands and ducts in multi-span post-tensioning structures is supposed to be minimal in the vicinity of the inflection points. Therefore, squeezing effect due to circular cross-section of ducts will only be concentrated in the vicinity of the vertices of parabolic tendons. However, a cylindrical post-tensioned concrete structure effectively has single curvature for the entire structure. Thus, strands are continuously in contact with the ducts over their full lengths. In that light, it is suggested that the squeezing effect could be exaggerated in curved post-tensioned concrete structures.

The arrangement of strands prior to the stressing likely remains the same after the stressing operation for the general post-tensioned concrete structures (Fig. 6). However, the prestressing strands in horizontally curved post-tensioning structures will be likely dragged toward the side of the duct during the prestressing operation, and could also be subjected to rearrangement of

the prestressing strand. The length of the prestressing strand will vary depending on the circumference resulting for the location of the strand within ducts, regardless of the inserting method (i.e. push-through and pull-through). Furthermore, when an individual strand is pushed through ducts of a large-angle post-tensioned structure, the prestressing strands could potentially be crossed which may lead to excessive binding during prestressing operations. These hypotheses are supported by the larger-than-anticipated friction losses obtained from test results.

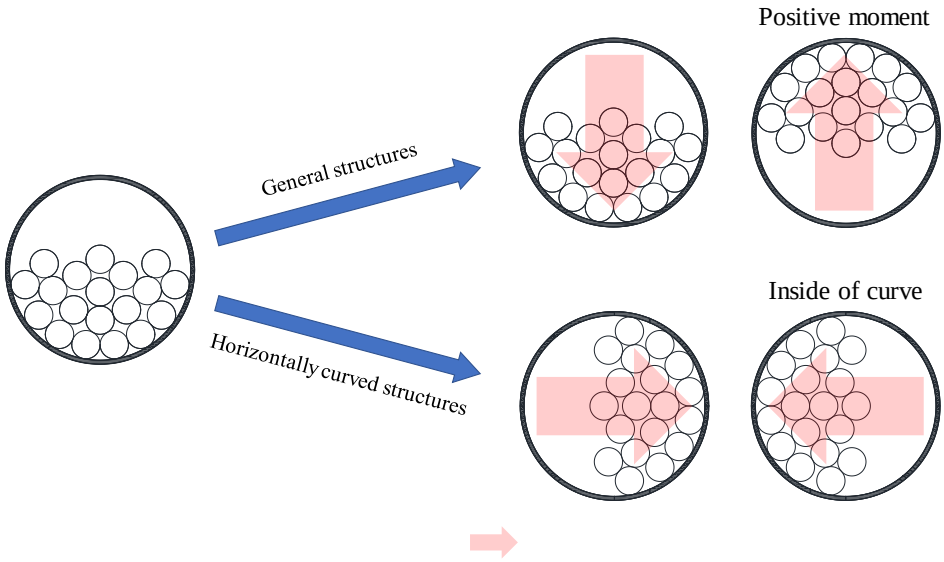

Fig. 6 Rearrangement of strands within a duct during prestressing operation

Therefore, the squeezing effect and the binding of prestressing strand which are typically negligible for general post-tensioned concrete structures could be exaggerated and result in larger friction losses for large-angle post-tensioned concrete structures.[8]

ELONGATION AND FRICTION COEFFICIENT

The tendon elongations and jacking forces should be recorded to verify the appropriate distribution of prestressing forces within the tendons. The jacking forces can be accurately measured using a well-calibrated pump; however, the measured elongation may be affected by several factors such as slack in the tendon, wedge seating, actual length of tendon, and so on.[15] To minimize such factors, initial forces are applied to the structures before measuring the elongation. Typically, an initial load ranging from 5 to 20 % of the final load are applied to the tendons for the purpose of removing slack. Then the elongation is measured as the tendons are loaded to the specified jacking force. The differences between measured elongation and expected elongation are expected to satisfy the tolerances specified codes[6,12] (Table 8).

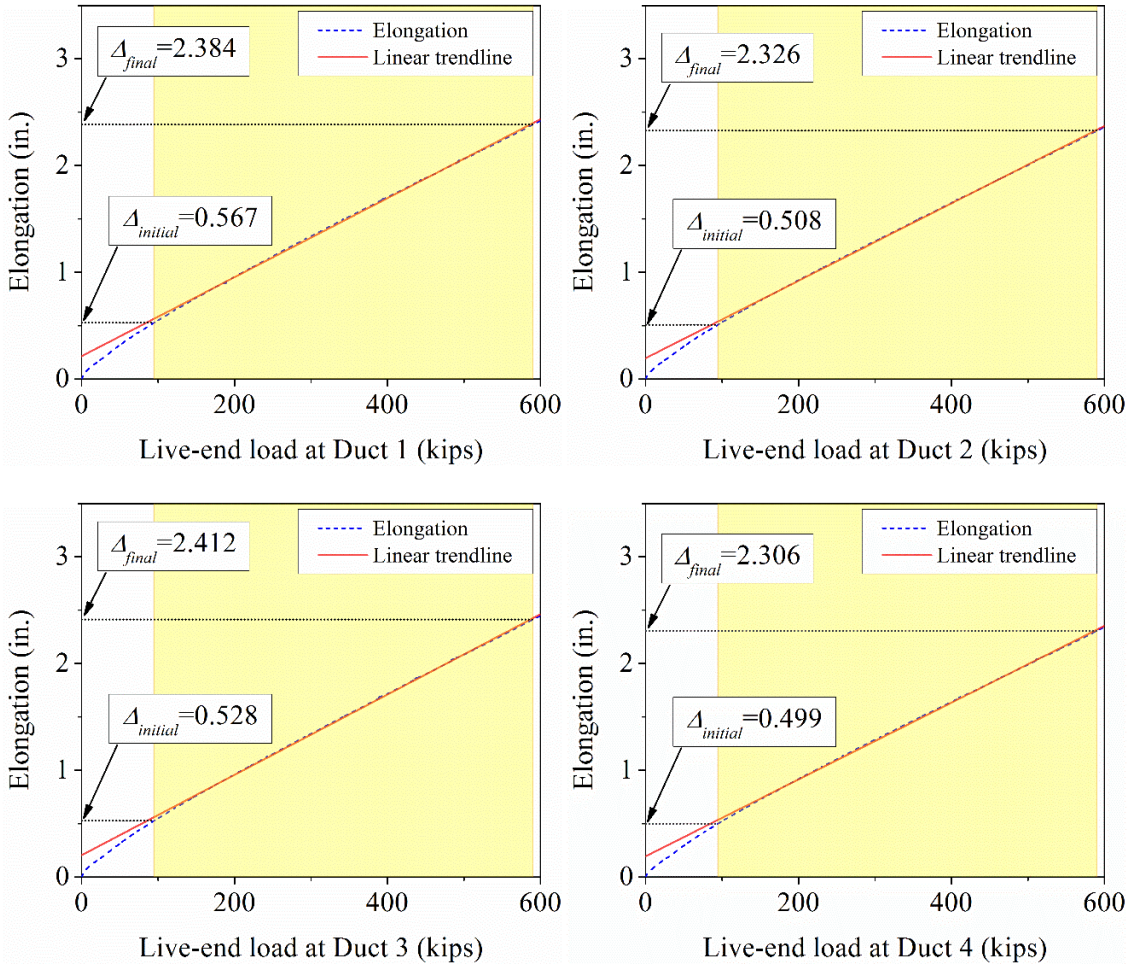

Fig. 7 Elongation of tendons at the initial load and the final load for Specimen 2. (Note: yellow shaded area is from $0.08f_{pu}$ to $0.50f_{pu}$)

For Specimen 2, the apparent elongations of tendons were obtained from the measured displacement of the stressing plate. A stress level of $0.50f_{pu}$ was assumed as a final load and 16 % of that final load ($0.08f_{pu}$) was selected as the initial load for Specimen 2. Even though a small load level (~ 2 kips) was applied in an effort to remove the slack from the tendons prior to commencing the stressing operation, the rearrangement of strands within the ducts may continue to occur. In Table 14, the measured elongations were compared with the expected elongations obtained using a curvature coefficient of 0.25, which was selected based on the types of duct and prestressing steel used in the testing program.[12] As shown in Table 14, the measured elongation of all tendons exceeded the 7 % tolerance specified by ACI 318-14[1]. Since actual curvature coefficients for each tendon were calculated, the expected elongations were recalculated and compared with measured elongations. As shown in Table 15, discrepancy between measured and estimated elongations for all tendons were within the tolerance limit of 7 %.

Table 14 Elongations using a curvature coefficient of $\mu = 0.25$

	Unit	Duct 1	Duct 2	Duct 3	Duct 4
Expected elongation ($\Delta_{calculated}$)	in.	1.848			
Apparent elongation at initial load ($\Delta_{initial}$)	in.	0.527	0.508	0.528	0.499
Apparent elongation at final load (Δ_{final})	in.	2.384	2.326	2.412	2.306
Measured elongation ($\Delta_{measured}$)*	in.	1.608	1.568	1.634	1.557
Error**	%	-13.0	-15.1	-11.6	-15.7
Tolerance requirement (7 %)		NG	NG	NG	NG

* $\Delta_{measured} = \Delta_{final} - \Delta_{initial} - \Delta_{slip}$; Δ_{slip} is a wedge slip assumed as 0.25;

** $\frac{\Delta_{calculated} - \Delta_{measured}}{\Delta_{calculated}} \times 100$

Table 15 Elongations using the respective curvature coefficients for each duct

	Unit	Duct 1	Duct 2	Duct 3	Duct 4
Expected elongation	in.	1.658	1.649	1.733	1.667
Apparent elongation at initial load ($\Delta_{initial}$)	in.	0.527	0.508	0.528	0.499
Apparent elongation at final load (Δ_{final})	in.	2.384	2.326	2.412	2.306
Measured elongation ($\Delta_{measured}$)*	in.	1.608	1.568	1.634	1.557
Error	%	-3.02	-4.89	-5.68	-6.59
Tolerance requirement (7 %)		OK	OK	OK	OK

It is interesting to note that the decreasing rate of expected elongations due to the increased curvature coefficients is less than the increasing rate of curvature coefficients. The curvature coefficients based on the measured loads were approximately increased from 0.25 to 0.40 (60 % increase) and the expected elongations were decreased from 1.861 to 1.677 in. (10 % decrease in average) accordingly. Since the method used to calculate the theoretical elongation is the same for all post-tensioned concrete structures, this trend can be also found in general post-tensioned concrete structures, regardless of the length of tendons and the geometry of the structures. It is possible that even though the jacking forces and elongation tolerances are satisfied with the specification, actual friction losses could deviate from anticipated friction losses. Therefore, if the force in the tendon is critical for the safety and serviceability of the structure, the force in the dead-end should be measured to verify design calculation.

CONCLUSIONS

The inaccurate estimation of the friction losses in some tendon geometries used in the post-tensioned concrete structure could lead to poor estimation of the force distribution within the structures and may cause a reduction in the actual versus required factor of safety and/or

serviceability problems. In this paper, friction losses and curvature coefficients of large-angle post-tensioned concrete wall assemblies were evaluated and several possible contributors of large friction losses were discussed. From this experimental program, several observations and conclusions can be made:

1. The range of curvature coefficients for 90-degree post-tensioning applications using 7-wire strands and smooth pre-bent metal ducts were determined to be: $\mu = 0.30$ to 0.50 if bundled strands were pushed-through, or $\mu = 0.50$ to 0.60 if individual strands were pushed-through.

2. Strand interactions (binding and squeezing effects), which are typically negligible for general post-tensioned concrete structures, are possible causes of large friction losses for large-angle post-tensioned concrete structures such as silos, bins, storages, and nuclear containments. Usage of the conventional friction coefficients for large-angle post-tensioned concrete structures could underestimate the actual friction losses and result in serviceability and reduction in the actual versus required factor of safety.

3. Even though the differences between measured and expected elongations may satisfy the tolerances specified in specifications, the dead-end loads may need to be measured after the prestressing operation to ensure proper distributions of tendon forces.

4. It is necessary to obtain more test data of curved post-tensioned concrete structures to generalize and develop reliable friction loss coefficients for large-angle post-tensioned concrete structures.

ACKNOWLEDGEMENTS

The authors acknowledge material donations from STRUCTURAL TECHNOLOGIES and Wire Mesh Corporation. The authors would like to thank the support staffs at the Ferguson Structural Engineering Laboratory at The University of Texas at Austin for their assistance during the construction and testing. The authors also thank Dean J. Deschenes for his valuable advice on the design and testing of the specimens.

REFERENCES

[1] ACI Committee 318, *Building Code Requirements for Structural Concrete and Commentary*, Farmington Hills, MI: American Concrete Institute, 1963 ~ 2014.
[2] AASHTO, *AASHTO LRFD Bridge Design Specifications*, Washington, DC: American Association of State Highway and Transportation Officials, 2014.
[3] fib, *fib Model Code for Concrete Structures 2010*, Lausanne, Switzerland: Wilhelm Ernst & Sohn, 2013.
[4] VSL, *Concrete Storage Structures - Use of the VSL Special Construction Methods*, Berne, Switzerland: VSL INTERNATIONAL LTD., 1983.

[5] DSI, "Multistrand Post-Tensioning System" Available: https://www.dsiamerica.com/products/post-tensioning-systems/strand-post-tensioning-system/installation/installation/.
[6] Post-Tensioning Institute, *Post-Tensioning Manual*, Phoenix, AZ: Post-Tensioning Institute, 2006.
[7] Lin, T. Y., "Cable friction in post-tensioning," *Journal of the Structural Division*, vol. 82, no. ST 6, Nov. 1956, pp. 1–19.
[8] Leonhardt, F., "Continuous Prestressed Concrete Beams," *Journal Proceedings*, vol. 49, no. 3, Mar. 1953, pp. 617–634.
[9] Jongkwon Choi, Clint R. Woods, Trevor D. Hrynyk, and Oguzhan Bayrak, "Behavior of Curved Post-Tensioned Concrete Structures without Through-Thickness Reinforcement," *ACI Structural Journal*, vol. 114, no. 4, Jul. 2017, pp. 983–994.
[10] Collins, M. P., and Mitchell, D., *Prestressed concrete structures*, Englewood Cliffs, N.J: Prentice Hall, 1991.
[11] ACI-ASCE Committee 343, *Analysis & Design of Reinforced Concrete Bridge Structures*, American Concrete Institute, 1995.
[12] ACI-ASCE Committee 423, *Guide to Estimating Prestress Losses*, Farmington Hills, MI: American Concrete Institute, 2016.
[13] Caltrans, *Bridge Design Specifications*, Sacramento, CA: California Department of Transportation, 2004.
[14] Cooley, E. H., *Friction in post-tensioned prestressing systems*, London: Cement and Concrete Association, 1953.
[15] Hayek, C., and Kang, T. H.-K., "Elongation Tolerance for Short Tendons in Post-Tensioned Building Structures," *Structural Journal*, vol. 114, no. 04, Jul. 2017, pp. 795–802.
[16] Clint Robert Woods, "Experimental Investigation of the Delamination Behavior of Curved Post-Tensioned Concrete Structures without Through-Thickness Reinforcement," Master thesis, The University of Texas at Austin, 2016.